Generation of multiciliated cells in functional airway epithelia from human induced pluripotent stem cells

Amy L. Firth[a], Carl T. Dargitz[a], Susan J. Qualls[a], Tushar Menon[a], Rebecca Wright[a], Oded Singer[a], Fred H. Gage[a], Ajai Khanna[b], and Inder M. Verma[a,1]

[a]Laboratory of Genetics, Salk Institute for Biological Studies, La Jolla, CA 92037; and [b]Department of Surgery, University of California, San Diego, CA 92013

Contributed by Inder M. Verma, February 26, 2014 (sent for review December 11, 2013; reviewed by Brigitte N. Gomperts and Konrad Hochedlinger)

Despite therapeutic advancement, pulmonary disease still remains a major cause of morbidity and mortality around the world. Opportunities to study human lung disease either in vivo or in vitro are currently limited. Using induced pluripotent stem cells (iPSCs), we generated mature multiciliated cells in a functional airway epithelium. Robust multiciliogenesis occurred when notch signaling was inhibited and was confirmed by (*i*) the assembly of multiple pericentrin-stained centrioles at the apical surface, (*ii*) expression of transcription factor forkhead box protein J1, and (*iii*) presence of multiple acetylated tubulin-labeled cilia projections in individual cells. Clara, goblet, and basal cells were all present, confirming the generation of a complete polarized epithelial-cell layer. Additionally, cAMP-activated and cystic fibrosis transmembrane regulator inhibitor 172-sensitive cystic fibrosis transmembrane regulator currents were recorded in isolated epithelial cells. Our report demonstrating the generation of mature multiciliated cells in respiratory epithelium from iPSCs is a significant advance toward modeling a number of human respiratory diseases in vitro.

differentiation | definitive endoderm | bronchi

Lung disease is the third highest cause of death in the United States after cardiovascular disease and cancer; however, unlike the latter two, death rates from pulmonary disease continue to increase. Modeling human lung disease currently requires the isolation of primary bronchial epithelial cells from the lungs of deceased patients. These lungs are often at the end stages of the disease and have been exposed to a variety of therapeutic approaches and environments. Furthermore, understanding the development of a genetic human lung disease, such as primary ciliary dyskinesia, is difficult to recapitulate accurately in vitro. A reproducible model of human lung disease from a self-renewing population of cells would create the opportunity to study human lung disease more extensively. Indeed, using homologous recombination to generate gene-corrected respiratory epithelial progenitor cells from a patient with genetic disease could proffer a potential therapeutic approach.

Generation of pluripotent stem cells from somatic cells [induced pluripotent stem cells (iPSCs)] has opened the door for creating patient- or disease-specific pluripotent cells with the potential to differentiate to disease-relevant cell types to model disease and screen for novel therapeutic approaches (1). To use such iPSCs to model lung disease, an effective differentiation protocol is necessary to generate pseudostratified polarized respiratory epithelium in a dish. In particular, this differentiation requires the generation of a specialized postmitotic multiciliated cell. The differentiation of embryonic stem cells and iPSCs to airway epithelial cells has recently received increased attention (2, 3). The current manuscript describes developing a differentiation protocol based upon lessons learned from embryogenesis to generate multiciliated cells (4–9).

Airway epithelium first develops from the definitive endoderm (DE). Both Wnt3a and activin A signaling are critical for the push from mesendoderm to DE, and a standardized protocol for the induction of DE from pluripotent stem cells is now widely accepted (10, 11). The anterior foregut endoderm (AFE), the caudal end that gives rise to the trachea and lung, can be subsequently induced from differentiated DE by inhibition of bone morphogenic protein (BMP) and transforming growth factor beta (TGFβ)/Nodal. This combination was shown to maintain forkhead box A2 (FOXA2) expression while augmenting the reemergence of sex determining region-Y box 2 (SOX2) (foregut marker) and suppressing the expression of hindgut marker caudal type homeobox 2 (12). BMP4 and fibroblast growth factor (FGF) are known to act downstream of Wnt3a and are involved in the differentiation and maintenance of the distal lung epithelium (13). FGF10 is expressed in the lung mesenchyme and is a critical regulator of endoderm proliferation and lung bud morphogenesis (14, 15). FGF7 [also known as keratinocyte growth factor (KGF)] can also be detected early in lung development and is known to interact with other factors to regulate epithelial branching and epithelial proliferation (16, 17). A combination of these factors in addition to the careful regulation of BMP4 expression can induce expression of the transcription factor NK2 homeobox 1 (NKx2.1) and push differentiation toward the ventral anterior endoderm (6, 18, 19). NKx2.1 is also known as thyroid transcription factor 1 (TTF-1) and is critical for the transcription of genes essential for thyroid and lung development. Thyroid cells can be defined by the acquisition of specific markers such as paired box 8 gene (PAX8), known to be important for thyroid epithelial cell differentiation and survival (20), and during development have also been shown to

Significance

Pulmonary disease is the third highest cause for morbidity and mortality worldwide. Studies of human lung disease in vivo or in vitro are currently limited. Using induced pluripotent stem cells, we developed a step-wise differentiation protocol ending in an air–liquid interface to generate a pseudostratified polarized layer of endodermal-derived epithelial cells (forkhead box protein A2$^+$ and NK2 homeobox 1$^+$). This layer includes Clara cells with Clara cell 10 kD-positive vesicles, mucin 5A/C-positive goblet cells, multiciliated cells, and isolated cells that have forskolin-induced chloride currents sensitive to cystic fibrosis transmembrane regulator inhibitor 172. The development of this model will enable the future study of many lung diseases (especially those where defective cilia are involved, such as primary ciliary dyskinesia) that have been difficult to study in human models from a developmental perspective.

Author contributions: A.L.F., F.H.G., and I.M.V. designed research; A.L.F., C.T.D., S.J.Q., T.M., and R.W. performed research; A.L.F., O.S., and A.K. contributed new reagents/analytic tools; A.L.F. analyzed data; A.L.F., T.M., F.H.G., and I.M.V. wrote the paper; and F.H.G. helped in setting up electrophysiology.

Reviewers: B.N.G., University of California, Los Angeles; K.H., Massachusetts General Hospital.

The authors declare no conflict of interest.

See Commentary on page 6120.

[1]To whom correspondence should be addressed. E-mail: verma@salk.edu.

This article contains supporting information online at www.pnas.org/lookup/suppl/doi:10.1073/pnas.1403470111/-/DCSupplemental.

lose expression of endoderm marker FOXA2 (21). Lung progenitor specification and lung maturation can be subsequently controlled by combinations of FGF, TGFβ, and BMP4 regulated signaling (3). In addition, the microenvironment can be critical to successful differentiation of cells; bronchial epithelial cells have been shown to differentiate into a mature polarized epithelium in vitro using an air–liquid interface model (22, 23).

Motile multiciliated cells (MCCs) are a population of specialized cells that have exited cell cycle and assembled basal bodies and that project hundreds of motile cilia as they differentiate. The notch signaling pathway is known to play critical roles in the maintenance and differentiation of stem cells, including basal cells in the adult lung (24). Recently, inhibition of notch has been shown to be essential for the development of MCCs in *Xenopus*, mouse, and human airways (24–30). Concentration-dependent notch signaling is known to be able to determine the fate of stem cells in both the mouse and human lung. Basal stem cells can undergo self-renewal, independent of notch, and then be driven to an early progenitor cell by the addition of notch. The fate of the progenitor cells is also determined by notch expression because lowest levels of notch signaling will push the cells toward a ciliated cell fate whereas higher concentrations will select for a secretory cell type (24).

This study demonstrates the differentiation of human iPSCs to MCCs that accumulate numerous pericentrin-labeled centrioles, allowing for the formation of multiple cilia projections in each cell. Only in the presence of notch inhibition was a substantial population of MCCs generated. Furthermore, we verify the robust pseudostratified polarized nature of the epithelial cells and demonstrate the presence of Clara cells with Clara cell 10 kD (CC10)-positive vesicles and mucin 5A/C (MUC5A/C)-positive goblet cells. Finally, we show the presence of forskolin-induced chloride currents sensitive to cystic fibrosis transmembrane regulator inhibitor 172 (CFTRinh-172) in isolated epithelial cells by the whole-cell patch-clamp technique. This model provides a platform for studying the development of lung diseases where cilia are defective, such as primary ciliary dyskinesia, or where secretory cells are deregulated, such as asthma and chronic obstructive pulmonary disease. With further purification, the model could be adapted for high-throughput compound screening for novel therapeutics for lung diseases, such as cystic fibrosis, asthma, and bronchitis.

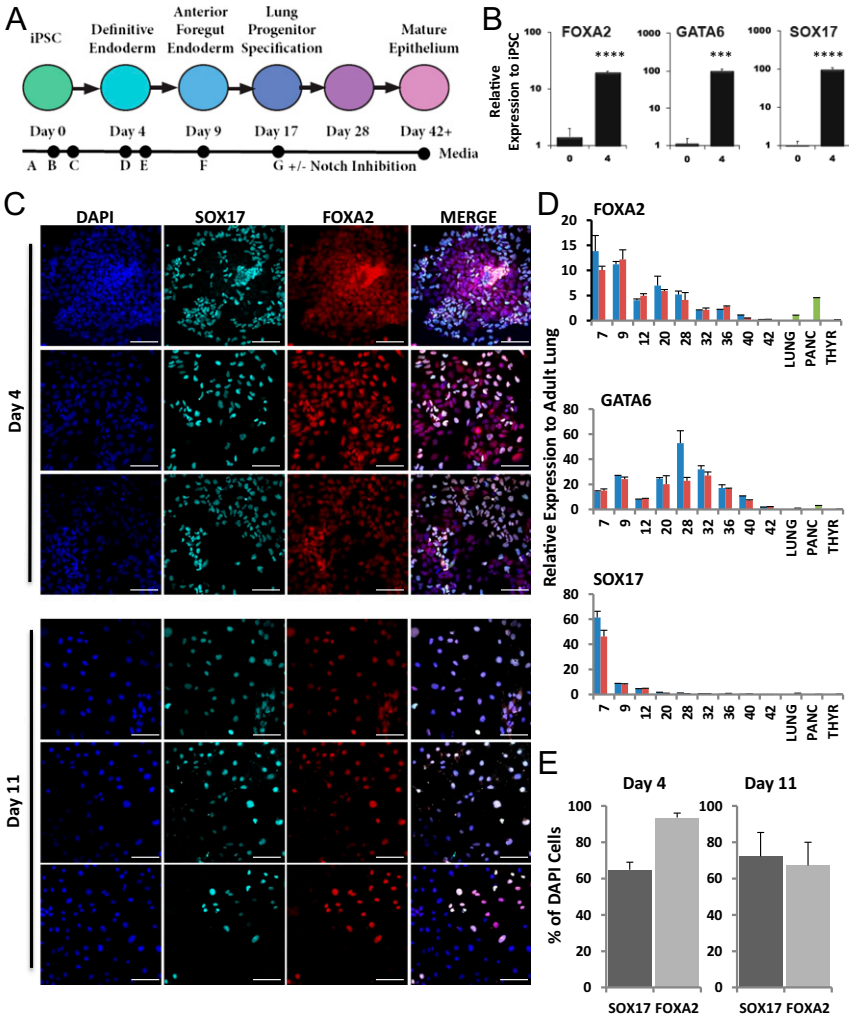

Fig. 1. Differentiation to definitive endoderm. (*A*) Summary of the differentiation protocol indicating the days of media changes (media are in *SI Appendix*, Table SII). (*B*) Up-regulation of FOXA2, GATA6, and SOX17 mRNA at day 4 of differentiation; data are normalized to iPSC. (*C*) Colocalization of SOX17 and FOXA2 at day 4 and day 11 of differentiation. (Scale bar: 100 μm.) (*D*) mRNA expression of DE markers over the time course of differentiation; data are normalized to whole adult lung cDNA. Red and blue bars represent two independent iPSC lines. (*E*) Quantification of the % of cells also expressing FOXA2 or SOX17 (mean ± SEM). $n = 6$ independent experiments. ***$P < 0.01$, ****$P < 0.001$.

Results

Generation of Airway Epithelial Cells. Induced pluripotent stem cells (iPSCs) were derived from human-skin fibroblasts using a polycistronic six-factor lentivirus, which was subsequently excised using CRE-recombinase (*SI Appendix, Supplemental Experimental Procedures* and *SI Appendix*, Figs. S1 and S2). The iPSCs were subjected to a stepwise differentiation protocol adapted from currently available protocols and based on normal lung development in utero (Fig. 1 and *SI Appendix*, Figs. S3–S7). The protocol follows basic stages of lung embryogenesis moving through a SOX17, FOXA2, and GATA binding protein 6 (GATA6) expressing definitive endoderm (Fig. 1 and *SI Appendix*, Fig. S3) and NKx2.1 expressing ventral anterior foregut endoderm (Fig. 2 and *SI Appendix*, Fig. S6). FOXA2 expressing DE was generated with a high efficiency of 93.6 ± 2.6%, with 64.8 ± 4.2% coexpressing SOX17 as can be seen in the representative images and quantification at day 4 of differentiation (Fig. 1 *C* and *E*). There was a concordant up-regulation of DE genes SOX17, FOXA2, and GATA6 at the mRNA level as shown for two independent cell lines in Fig. 1*B*. DE also triple stained for epithelial calmodulin (EpCAM), tyrosine-protein kinase Kit (C-KIT or CD117), and C-X-C chemokine receptor type 4 (CXCR4 or CD184), with >99% of cells double-positive for EpCAM and CXCR4 and ∼45% triple-positive with C-KIT expression also at day 5 of differentiation; by day 9, the triple-positive population had increased to ∼70% (*SI Appendix*, Fig. S4). By day 11 of differentiation, 67.2 ± 12.7% of cells expressed FOXA2 and 72.3 ± 13.1% SOX17, indicating efficient differentiation to DE, which is maintained through the anterior foregut endoderm and lung endoderm differentiation stages (Fig. 1*E*). Over the time course, the mRNA expression of these DE markers gradually decreased to levels comparable with adult lung (Fig. 1*D*).

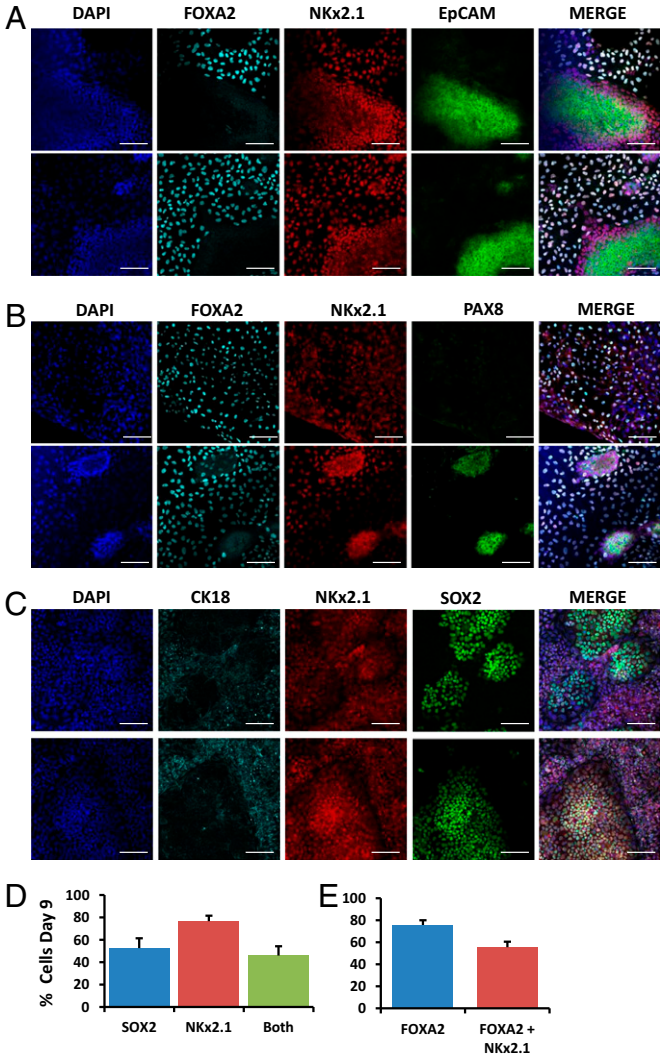

Fig. 2. Anterior foregut endoderm specification. Representative immunofluorescent images of day 9 of differentiation indicating the colocalization of FOXA2, NKx2.1, and EpCAM (*A*) or PAX8 (*B*). (*C*) The same time point stained with CK18, NKx2.1, and SOX2. (*D*) The % of the DAPI cells stained with SOX2, NKx2.1, or both and (*E*) the % of the DAPI cells stained with FOXA2 or FOXA2 and NKx2.1 at day 9 of differentiation (mean ± SEM). $n = 7$ independent experiments. (Scale bar: 100 μm.)

Inhibition of BMP and TGFβ signaling on day 5 of differentiation, followed by continued TGFβ inhibition with the addition of BMP4 on days 6–9, was used to push the DE to differentiate to ventral anterior foregut. By day 9, there was a notable population of cells that strongly expressed EpCAM and NKx2.1 but had lost the expression of FOXA2 (Fig. 2*A*). It is likely that this population of cells represents the development of a thyroid lineage. Although we do not observe nuclear PAX8 staining, nor mRNA expression of PAX8 or thyroid-stimulating hormone releasing hormone, we did observe some thyroglobulin (Tg) expression, which would indicate that a population of thyroid-like cells are generated in our protocol (Fig. 2*B* and *SI Appendix*, Fig. S5*B*). By day 9, $FOXA2^+NKx2.1^+$ cells also expressed EpCAM. Foregut endoderm can also be identified by costaining with SOX2; at day 9 of differentiation, 52.5 ± 8.2% of cells expressed SOX2, with $NKx2.1^+SOX2^+$ cells representing 45.9 ± 8.4% of DAPI-expressing cells. $NKx2.1^+$ cells could also represent a population of ventral forebrain progenitors (Fig. 2 *C* and *D*); although there was some scattered Tuj1 expression in the derived epithelial cells at day 9 of differentiation, it did not account for the majority of the $NKx2.1^+$ cells (*SI Appendix*, Fig. S6*A*). In the anterior foregut endoderm, 75.7 ± 4.2% expressed FOXA2, with 55.6 ± 5% coexpressing NKx2.1 ($n = 12$) (Fig. 2*E*). Pancreatic endoderm marker paired box protein 6 decreased in expression compared with the control, undifferentiated iPSCs, after 45 d of differentiation, indicating minimal differentiation to pancreatic endoderm (*SI Appendix*, Fig. S9*A*). It is worth noting that currently available in vitro differentiation lung progenitor differentiation protocols have also observed contamination of the lung endoderm differentiation with thyroid, neuronal, and mesodermal differentiation (31, 32).

The concentration of BMP4 in lung development is known to be tightly regulated so we investigated changes in the BMP4 concentration during the early stages of differentiation (protocol from days 5–17). Zero, 5, and 20 ng/mL were used, and RNA was collected from the differentiation at day 45. Analysis of lung-related gene expression at this time point showed that 5 ng/mL supported the most robust up-regulation of genes related to lung development and mature lung cells, such as DE makers FOXA2, GATA6, goblet cell marker MUC5A/C, MUC1, CFTR, and transcription factor cEBPα (important for lung-branching morphogenesis) (33, 34), and was thus used as the working concentration for the protocol (shown in *SI Appendix*, Fig. S7). Analysis of the cells by FACS at day 10 of differentiation indicated ∼70% $EpCAM^+$ cells, with ∼28% expressing mesenchymal marker cluster of differentiation factor 90 (CD90) (Thy-1) (*SI Appendix*, Fig. S8*A*). This data indicates that, by day 10 of differentiation, a population of the cells pushed to definitive endoderm had assumed a mesenchymal phenotype.

Maturation of the primed airway epithelial progenitor cells was induced at day 17 by allowing the cells to be maintained in an air liquid interface (ALI), reflecting more closely the environmental niche of mature epithelial cells in the lung. Such an ALI is commonly used to push the maturation of human primary

bronchial epithelial cells in vitro and has been used to assist in the differentiation of embryonic stem cells to lung epithelial cells (2, 35, 36). The ALI was maintained in media G on the basolateral side (37) and used to promote maturation and polarization of the epithelial cell layer.

Functional epithelial cell layers are characterized by the development of tight junctions between cells forming a high-resistance epithelial barrier (38). The expression of tight junction protein ZO-1 (also known as occludin-1), epithelial cadherin (E-Cadherin) (both a marker of epithelial cells and a cell-adhesion molecule), and epithelial calmodulin (EpCAM) was observed at the cell junctions [Fig. 3*A*, shown at day 45 of differentiation (day 28 of ALI)]. Polarization of the mature airway epithelial cells is essential to their function; concentration gradients are established for nutrients and growth factors, the basal side is adapted for anchorage, and the apical side is adapted for cell-specific functions. Analysis of our epithelial cell cultures after 45 d of differentiation indicated cuboidal-shaped polarized cells (Fig. 3*B*). The expression of epithelial markers cytokeratin 18 (CK18), EpCAM, and E-Cadherin was localized to the apical epithelial layer, and staining clearly shows the tight junctions between cells (Fig. 3*C*). Our differentiation protocol generates a supportive mesenchyme layer with a polarized layer of epithelial cells only on the most apical side. Mesenchymal markers vimentin and CD90 localized to the layers of cells underneath the apical epithelial cell layer (Fig. 3*D*) suggest the possibility of a niche supporting epithelial differentiation. The precise role for this supportive mesenchymal cell layer requires further investigation; however, it was notable that, if cells were first differentiated in a dish and then transferred to the transwells, this layer did not robustly form and the terminal differentiation did not efficiently generate the desired mature epithelial cell types. This observation is supported by quantitative polymerase chain reaction (qPCR) data for two independent iPSC lines comparing plating at day 0 and day 8 of differentiation onto the transwells and the substantial drop in expression of Clara, goblet, and basal cell genes (*SI Appendix*, Fig. S9). Furthermore, cell density at the endpoint (day 45) was much lower and less 3-dimensional, with fewer FOXA2 and SOX2 positive cells (*SI Appendix*, Fig. S9*B*).

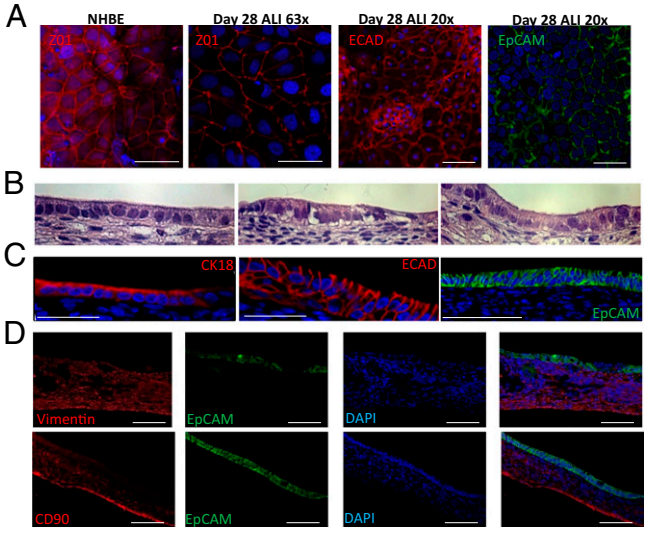

Fig. 3. Generation of pulmonary epithelium. (*A*) Differentiated normal human bronchial epithelial (NHBE) cells stained with ZO-1 (red). iPSCs at day 28 of differentiation stained with ZO-1 (red), epithelial cadherin (ECAD, red), and epithelial calmodulin (EpCAM, green). Images shown at 63x as labeled. (Scale bar: 50 μm.) Images shown at 20x as labeled. (Scale bar: 100 μm.) (*B*) H&E-stained histological samples showing a cuboidal layer of epithelial cells on the apical surface. (*C*) Staining of the apical cell layer with CK18 and ECAD (red). (Scale bar: 50 μm.) Staining of the apical cell layer with EpCAM (green). (Scale bar: 100 μm.) (*D*) Images showing the mesenchymal layer stained by CD90 and vimentin (red) and the epithelial layer stained with EpCAM (green). (Scale bars: 100 μm.) Nuclei are counterstained with DAPI (blue) in all images.

By day 45 of differentiation, the EpCAM-positive cells represented 40–55% of the cells, with the majority (>80%) coexpressing CD44. $CD90^+$ mesenchymal cells represented 17–40% of the final population. Representative FACS plots are shown in *SI Appendix*, Fig. S8 for control and conditions where γ secretase was inhibited using either N-[(3,5-difluorophenyl)acetyl]-L-alanyl-2-phenyl]glycine-1,1-dimethylethyl ester (DAPT) or Ly441575 to inhibit notch and push ciliogenesis. After 45 d of differentiation (25 d in the ALI), $FOXA2^+$, $NKX2.1^+$ cells were still observed in the apical cell layer (*SI Appendix*, Fig. S10*A*). $FOXA2^+$ cells also displayed nuclear localization of p63 (*SI Appendix*, Fig. S10*B*), and the quantity of p63-positive cells in this section may indicate airway progenitors in a currently nonpseudostratified region of the differentiation. Sections showing apical to basolateral organization indicated an epithelial cell layer where CK18 and NKx2.1, and tumor protein p63 and CFTR were colocalized (*SI Appendix*, Fig. S10 *C* and *D*, respectively). Basal cell markers p63, nerve growth factor receptor, and Kertatin 5 all increased in mRNA expression over the time course of differentiation, peaking between 11 and 18 d in the air–liquid interface and returning to levels similar to those observed in whole adult lung lysate after 45 d of differentiation (*SI Appendix*, Fig. S10*E*).

Formation of Multiciliated Cells. Proximal airway function relies upon the cells having multiple motile cilia to generate a flow in the periciliary layer and keep mucus moving over the airway surface. Ciliated cells beat to propel mucus produced by secretory cells, such as Clara and goblet cells, out of the airway (39, 40). This mucociliary clearance protects the airway from infection. Forkhead box protein J1 (FOXJ1) is a transcription factor associated with the activation of genes necessary for the anchoring of basal bodies at the apical surface and initiating ciliogenesis (41, 42). In our differentiation protocol, FOXJ1 gene expression is highly up-regulated after switching to ALI at day 17 following initiation of differentiation (Fig. 4*B*). Analysis by confocal microscopy indicated that FOXJ1 expression is localized in the nucleus (Fig. 4 *A* and *C*). Pericentrin is known to be associated with both centrioles at the base of primary cilia and motile cilia (43). After 28 d in ALI, confocal analysis of cilia suggests that the majority of ciliated cells are in the early stages of multiciliogenesis. Small clusters of pericentrin foci are visible along with associated acetylated alpha tubulin-stained cilia projections; however, under these control differentiation conditions, little evidence for true multiciliogenesis was found (Fig. 4*D*). We believe that these cells represent cells that are not fully differentiated. It has been shown that primary cilia are found transiently in the airways but not in well-differentiated airway epithelium. In addition, primary cilia have been observed in the luminal layers of epithelium and basal cells after lung injury (44). Inhibition of notch signaling is known to be involved in the switch from a primary ciliated cell to an MCC (24, 27, 28, 45). DAPT inhibits notch signaling via its action on γ secretase. When DAPT was added at day 1 of ALI (experiment day 17) and maintained in the media for the following 28 d, MCCs were observed (Fig. 4*E*). These cells show the assembly of multiple cell bodies (indicated by staining with pericentrin) and multiple cilia projections (indicated by acetylated tubulin staining). Inhibition of notch signaling, with either γ secretase inhibitors DAPT and LY441575 or notch transcription factor inhibitor SAHM-1 enhanced the mRNA expression of genes related to the formation of

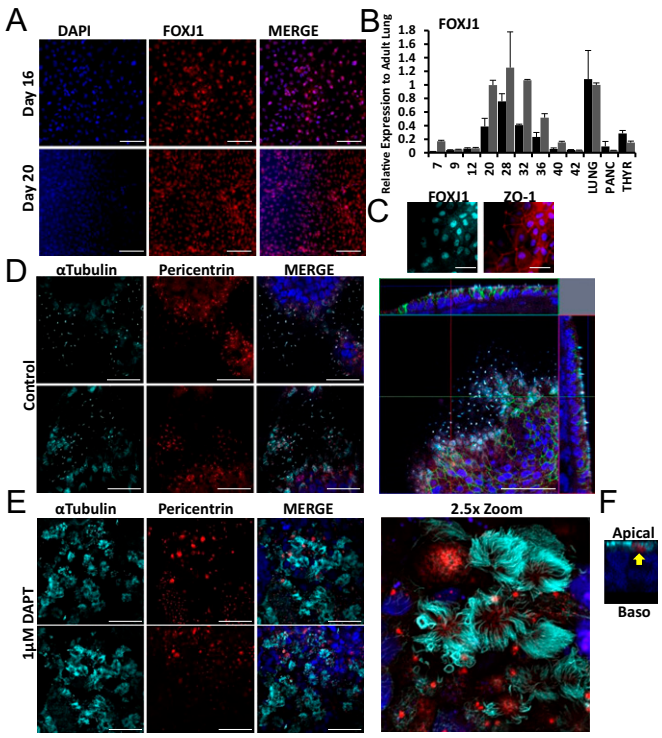

Fig. 4. Generation of MCCs with Inhibition of notch signaling. (*A*) Representative images showing colocalization of FOXJ1 and DAPI at days 16 and 20 of differentiation. (Scale bar: 100 μm.) (*B*) qPCR for FOXJ1 expression during differentiation. Data are shown for two primer sets (gray/black) and are corrected for internal control GAPDH and normalized to whole-lung cDNA. Data are expressed as mean ± SEM and represent $n \geq 2$ repeats per cell line. (*C*) Expression of transcription factor FOXJ1 (cyan); nuclei are counterstained with DAPI (blue) and cells indicated with ZO-1 (red). (Scale bar: 50 μm.) Representative images of cilia in the absence (Control) (*D*) and in the presence (DAPT-treated) (*E*) of notch inhibition. (Scale bar: 50 μm.) Cilia are indicated by acetylated alpha tubulin (cyan) and centrosome assembly by pericentrin (red), and nuclei are counterstained with DAPI (blue). *D*, *Right* indicates the three planes of view showing primary cilium at the apical surface and *E*, *Right* shows a 2.5× digital zoom image of multiciliated cells with dense centrioles marked with pericentrin. (*F*) The apical localization of both the cilia and the pericentrin (yellow arrow).

functional cilia (*SI Appendix*, Fig. S11*A*) compared with the vehicle control (DMSO). Although dynein axonemal assembly factor 1, dynein axonemal heavy chain 9, and dynein axonemal intermediate chain 1 were barely detected, it should be noted that the normal human bronchial epithelial (NHBE) cell levels were comparable with the iPSC differentiation experiment. Although the precise roles and functions of these genes will need further investigation, we can currently conclude that the generation of multiciliated cells and the expression of genes associated with ciliogenesis are increased under conditions where notch signaling is reduced.

Generation of Secretory Cells. Function of the respiratory epithelium also relies upon Clara and goblet cells to secrete proteins that maintain the function of the periciliary layer (46, 47). Goblet cells are glandular columnar cells more localized in bronchi that secrete mucin; MUC5A/C is the gene that encodes Mucin 5AC and is associated with goblet cells in the respiratory epithelium (48). Clara cells are nonciliated secretory epithelial cells lining the pulmonary airways that secrete Clara cell secretory protein (CCSP) (also known as CC10, CC16, or uteroglobin) (49). Clara cells were identified during differentiation from iPSCs by the expression of CC10 in vesicle-like structures on the apical surface of the epithelial layer (representative images are shown in Fig. 5 *A* and *B*). CC10 mRNA expression increased over the time course of differentiation, and the protein also colocalized with the nuclear expression of NKx2.1 (Fig. 5*B*); and the data in *SI Appendix*, Fig. S10 show that nuclear expression of NKx2.1 at this time point was associated with colocalization of FOXA2, indicating that the CC10-expressing cells were derived from lung-specific endoderm. Clara cells represented 27.3 ± 3.7% ($n = 4$ independent experiments) of the differentiated epithelial cell layer. Goblet cells were similarly identified by staining with MUC5A/C and represented a much smaller fraction of the cells (~1–2% on average) (Fig. 5*C*). The relative distribution of these Clara cells is representative of in vivo airways where they represent 0.4% of cells in the trachea, increasing up to 22% in the bronchioles (46). Goblet-cell distribution is <2% in the large airways of mice but is often higher in human airways, dependent upon exposure to environmental factors. Up-regulation of MUC5A/C, MUC1, and transcription factor SAM pointed domain containing ETS transcription factor (SPDEF), required for goblet-cell differentiation (50), was seen during differentiation (*SI Appendix*, Figs. S7 and S9). As previously mentioned, the detection of MUC5A/C was dependent upon the day the cells were transferred to the inserts. Analysis day 45 of differentiation indicated that cells directly seeded onto the inserts at day 0 of differentiation had increased mRNA expression of secretory cell markers (SPDEF, MUC1, and MUC5A/C) compared with transfer at day 8 (*SI Appendix*, Fig. S9). Pulmonary surfactant comprises lipids and proteins that are important for maintaining the surface tension at the air–liquid interface in the lungs (51). They are primarily secreted by alveolar cells; however, they are also detected in and secreted by Clara cells and alveolar macrophages (52, 53). We observed expression of surfactant protein D at the apical surface of the epithelial cells (Fig. 5 *D* and *E*).

Functional Expression of CFTR. Maintenance of the periciliary layer is also dependent upon the functional expression of CFTR

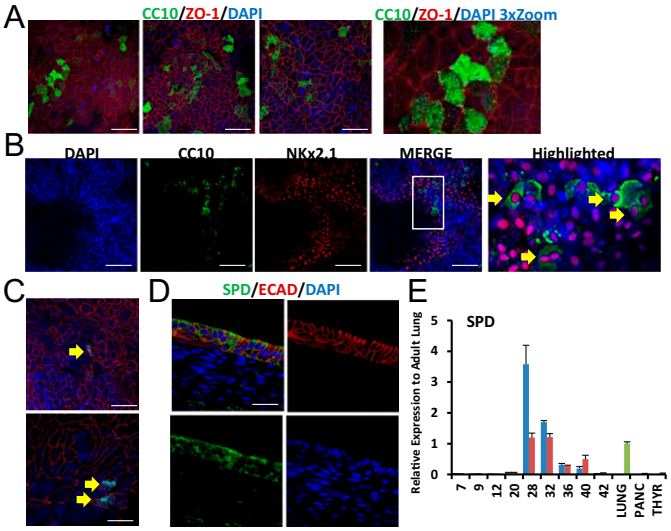

Fig. 5. Generation of secretory cells. (*A*) Representative images of iPSC-derived CC10-expressing cells (green), ZO-1 (red), and nuclei (blue). (*B*) Images at day 45 indicating the colocalization of CC10 (green) with NKx2.1 (red). (*C*) Representative images showing the generation and frequency of MUC5A/C (cyan) stained cells (indicated by the yellow arrows). (*D*) Representative images of the apical epithelial layer stained with surfactant protein D (SPD) (green), ECAD (red), and DAPI (blue). (*E*) qPCR expression of SPD over the differentiation time course normalized to whole adult lung cDNA. Red and blue bars represent two independent iPSC lines. (Scale bars: *A*–*D*, 100 μm; *E*, 50 μm.)

localized to the apical membrane. CFTR could be visualized at the apical surface of polarized cells in the ALI (Fig. 6*A*). Expression of CFTR at the mRNA level was observed throughout the differentiation after specification of the pulmonary endoderm stage (*SI Appendix*, Figs. S7 and S9). Although the exact nature of an interaction between CFTR and the epithelial sodium channel, ENaC, is still debated, it is generally agreed that there is an interaction between the two (54). ENaC was observed during differentiation at the apical surface of the polarized cells and at the cell membrane (Fig. 6*B*). After 45 d of differentiation, cells were dissociated and plated on collagen IV-coated plates and passed for three passages before preparation on coverslips for patch-clamp experiments. At day 45, 40–55% of cells expressed EpCAM (*SI Appendix*, Fig. S6*B*), and, after two passages in bronchial epithelial growth media (BEGM), cells maintained homogenous epithelial cell morphology (Fig. 6*E*). CFTR function was assessed by whole-cell patch-clamp studies in conditions where K^+, Na^+, and Ca^{2+} currents were minimal. Activation of CFTR by the addition of 10 μM forskolin, a c-AMP analog, showed an increase in the current that was subsequently reversed to baseline by CFTRinh172 (Fig. 6*C*). Fig. 6*C*, *Right* shows the CFTRinh172-sensitive chloride current. The IV curve indicates a significant increase in the forskolin-stimulated current at voltages positive to +40 mV. It should be noted that 2 of 10 cells did not respond to forskolin, indicating that not all cells isolated in the mixed epithelium culture expressed CFTR protein.

Discussion

We describe the differentiation of human iPSCs to a functional epithelium containing multiciliated, Clara, goblet, and basal cells in a polarized layer with functional CFTR activity analogous to that observed with mouse iPSCs (32, 55).

Multiciliated cells (MCCs) are a very specialized cell type in which hundreds of centrioles are generated in postmitotic progenitor cells. Centrioles form the core of the centrosome and are a microtubule-based structure that anchors the cilium (56). The generation of MCCs is critical to the function of a respiratory epithelium; their coordinated beating is essential for the movement of mucous and protection of the lung. Generation of robust MCCs from human iPSCs (Fig. 4) provides the opportunity for in-depth study of the development of these cells in the human system and may lead to the discovery of new mechanisms and therapeutic approaches for diseases, such as primary ciliary dyskinesia (PCD), that have been difficult to model and understand with the research tools currently available (57).

The influence of notch signaling on epithelial cell differentiation is well documented, and its level of expression is known to influence the maturation of these cells (24, 26–28, 45, 58). In our differentiation model, only in the presence of notch inhibition were true MCCs evident. It is interesting to note that, at day 28 of ALI (day 45 of differentiation), there are cells in the presence of notch inhibition that show the assembly of multiple basal bodies but do not have cilia projections. It is possible that the level of notch inhibition and the time undergoing differentiation are factors influencing this formation of cilia projections, but further investigation will be required.

Our current protocol not only has the capacity to up-regulate the mRNA indicative of differentiation to the various cell types of the respiratory epithelium, but also shows evidence for the appropriate distribution of these cells throughout the in vitro generated epithelial cell layer. The Clara cells show CC10 distributed

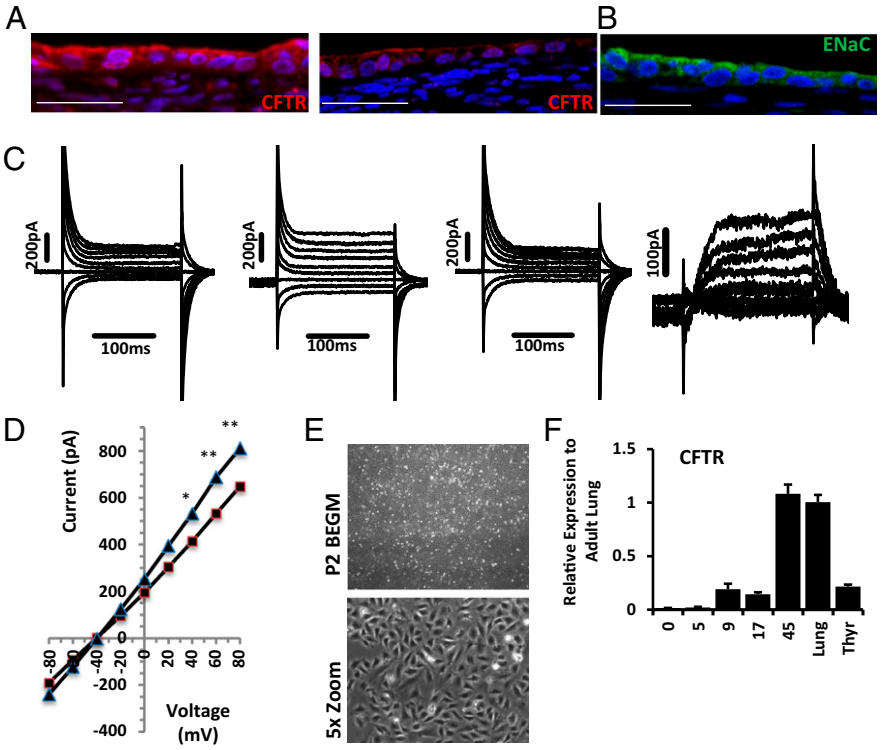

Fig. 6. Functional CFTR expression at the apical surface. (*A*) CFTR (red) expression at the apical surface; nuclei are counterstained with DAPI (blue). (Scale bar: 50 μm.) (*B*) Apical expression of ENaC (green). (Scale bar: 50 μm.) (*C*) Representative whole-cell chloride currents recorded from −80 to +80 mV in 20-mV increments at baseline and in the presence of forskolin and forskolin plus CFTRinh-172. (*Right*) Traces represent the CFTRinh-172–sensitive current. (*D*) I/V curves for baseline (squares) and in the presence of forskolin (triangles). $*P < 0.05$, $**P < 0.01$ (paired *t* test). (*E*) Phase images indicating the morphology of the expanding cells at P2 used for the patch-clamp experiments (20x and magnified 5x). (*F*) mRNA expression of CFTR over a time course of differentiation; data are corrected for GAPDH and normalized to whole-lung cDNA ($n = 6$).

in large secretory vesicles while retaining their NKx2.1 and FOXA2 expression (59). The goblet cells, although infrequent in number, also demonstrate specific expression of MUC5A/C, which does not colocalize in the CC10-expressing cells (Fig. 5) (60). The research preceding the Rossant study (2) focused primarily on the differentiation of mouse pluripotent cells and demonstrated the generation of lung progenitor cells (3, 32). There are significant differences in mouse-lung morphology and disease development. While providing some very important information, mouse models of diseases such as asthma and cystic fibrosis do not accurately represent the human disease (61, 62). The aforementioned reasons highlight the importance and necessity for a pliable human model of lung disease. The differentiation protocol featured in the current manuscript provides a platform for the study of many human respiratory diseases, such as asthma, PCD, and inflammatory diseases, in a dish.

The robust generation of a mature layer of epithelial cells also generated a mesenchymal layer on the basolateral side. Similar observations were made in a protocol describing the efficient generation of ATII cells (31). When differentiating cells were plated at later time points on the inserts, the capacity for generation of a good pseudostratified epithelial layer was reduced. It will be essential to determine what this mesenchymal layer provides in its "environmental niche" to support the epithelial differentiation. This mesenchymal layer is also somewhat problematic when trying to measure transepithelial electrical resistance (TEER). It caused the cells to pull away from the edges of inserts, thus reducing TEER. With regards to TEER development, it is also worth noting that, in cultures of primary human bronchial epithelial cells and immortalized cell lines, variability in the development of TEER does exist and that the Ev-Ohm meter has a tendency to underestimate actual resistance (63, 64). We are currently working on methods to isolate specifically the lung epithelial cells to also make this a reproducible model for high-throughput screening.

Our work describes a method to generate a renewable source of human epithelial cells, including multiciliated cells, that can be used to study human respiratory diseases that have previously been difficult to study and model in vitro. Human iPSCs provide an unlimited source of cells and also proffer the opportunity for gene editing and clonal expansion of cells for disease modeling. There are several lung diseases with a known genetic origin, such as cystic fibrosis and PCD, that could be corrected by replacement of the defective gene with the correct gene by gene-editing technology (65). It is hoped that, eventually, patient-specific iPSC cells can be used in this model, not only to provide a platform for understanding the cellular and molecular mechanisms of the disease, but to generate a gene-corrected transplantable cell type capable of engraftment into the lung.

Methods

Isolation of Patient Fibroblasts and iPSC Generation and Characterization. Data are included in *SI Appendix, Supplemental Experimental Procedures*.

Flow-Activated Cell Sorting. Cell surface markers of iPSCs were quantified using SSEA4, Tra-1-81, and Tra-1-60 (*SI Appendix*, Table SI). Cells were prepared by resuspension as single cells, using Accutase, incubated at 4 °C for 30 min in fluophore-conjugated antibodies, before washing in flow-activated cell sorting buffer [PBS with 2% (vol/vol) FBS], filtering (40 μm), and analysis on an LSR II flow cytometer (BD). Data were exported and analyzed using FlowJo software. For epithelial cell analysis, a single-cell suspension of live cells was isolated and stained with EpCAM-AF488, CD90-PE, and CD44-AF647 for 30 min on ice followed by 2× washes. Dead cells were stained with 7-AAD and gated out on the PerCP channel on the LSR II.

Immunocytochemistry. Cells were fixed in 3.2% (vol/vol) paraformaldehyde for 10 min at room temperature or overnight at 4 °C, washed 3× with PBS, and permeabilized in 0.5% Triton X-100 for 5 min at room temperature. Cells were blocked for 1 h with 2% (wt/vol) BSA (Sigma-Aldrich) and 5% (vol/vol) normal donkey serum (Jackson Immunoresearch) in PBS and then incubated in primary antibody at 4 °C overnight. Cells were washed 3× in PBS and incubated for 1 h in secondary antibodies raised in donkey (*SI Appendix*, Table SI). Stained cells were finally incubated in DAPI for 5 min before washing and mounting on glass microscope slides in Fluomount-G. Images were taken at either 20× or 63× on a Zeiss LSM 710 confocal microscope and processed/counted using Image J.

Immunohistochemistry. Paraffin-embedded sections were deparaffinized by washing for 3 × 5 min in xylene, 2 × 10 min in 100% EtOH, 2 × 10 min in 95% (vol/vol) EtOH, and 2 × 5 min in ddH_20. Antigen retrieval buffer was preheated to 90 °C, and the slide was incubated for 30 min and then allowed to cool for 20 min. The slides were blocked in 1× PBS with 5% (vol/vol) normal donkey serum and 0.3% Triton X-100 for a minimum of 1 h before staining in primary antibody overnight at 4 °C.

Epithelial Monolayer Histology. Differentiated epithelial cells on inserts were fixed overnight at 4 °C in 3.2% paraformaldehyde for 24 h and transferred to 70% ethanol for storage. The membranes were carefully cut from the holder using a clean razor blade and placed into a plastic cryomold containing a warmed solution of 1% Agarose. Once cooled, the agarose-embedded membrane was removed from the mold and routinely processed on a Shandon Excelsior Tissue Processor for paraffin embedding. Before paraffin embedding, the membrane was sliced into strips that were embedded standing on edge for cross-sectioning at 5 μm on a rotary microtome.

Differentiation to Airway Epithelial Cells. Differentiation followed a stepwise protocol. Transwell inserts were coated with a combination of fibronectin (5 μg/mL; BD Biosciences), laminin (5 μg/mL; Sigma-Aldrich), and collagen IV (60 μg/mL; Sigma-Aldrich), or six-well plates were coated with Matrigel. A single-cell suspension of iPSCs was generated using TrypLE (Life Technologies). Then, 300,000 iPSCs were plated per 30-mm insert or 120,000 per 12-mm insert in TeSR with ROCK inhibitor for 24 h. Differentiation to definitive endoderm consisted of 1 d in RPMI with 100 ng/mL activin A and 25 ng/mL Wnt3a (medium B) and 2 d in RPMI with activin A (100 ng/mL) and 1% FBS (medium C) (10, 11). This definitive endoderm step was followed by an anterior foregut endoderm push (media D and E) and a push for lung-specific endoderm (medium F) (*SI Appendix*, Table SII). Cells were then differentiated into a mature pseudostratified airway epithelium in an air–liquid interface (ALI). The ALI medium (medium G) is included in *SI Appendix*, Table SII.

Quantitative PCR. Total RNA was isolated from one well per insert of cells using the Qiagen Easy RNA mini kit as per the manufacturer's protocol. Then, 500 ng of RNA was DNase treated (Ambion) as per the manufacturer's protocol and then reverse-transcribed to cDNA using a High Capacity cDNA kit (Applied Biosystems). Quantitative PCR was performed using SYBR Green (Applied Biosystems) in a 5-μl reaction volume at 50 °C for 2 min, 95 °C for 10 min, 95 °C for 15 s, 60 °C for 1 min, 40 cycles and analyzed using 7900HT SDS software (Applied Biosystems). Each run was carried out, at minimum, in duplicate for three samples per experiment. GAPDH was used as an internal control. The data were then either normalized to iPSC or human whole-lung cDNA (as indicated in Figs. 1–6). Data are expressed as normalized cycle threshold (ct) ± SEM and represent an average of two to three repeats minimum of three experimental replicates. Whole-lung, thyroid, and pancreas cDNA were used as controls. Primers used for qPCR are included in *SI Appendix*, Table SIII.

Patch-Clamp Electrophysiology. Cells were resuspended using Accutase and plated on collagen IV-coated wells in BEGM (ATCC) for two passages and then split onto 12-mm round glass coverslips coated with Matrigel for patch-clamp experiments. For CFTR recording, the pipette (intracellular) solution contained (in mM): NaCl 5, $MgCl_2$ 2, CsCl 145, EGTA 10, Hepes 10, MgATP 5 (CsOH to pH 7.2). The bath (extracellular) solution contained (in mM): $CaCl_2$ 2, NaCl 150, $MgCl_2$ 2, Hepes 10 (Tris·HCl to pH 7.4). Cells were held at a holding potential of −40 mV, and 200-ms depolarizing steps in 20-mV increments from −80 to +80 mV were applied using an Axopatch 200B amplifier (Molecular Devices). The data were filtered at 2 kHz and digitized at 4 kHz. Cell capacitance and series resistance were routinely monitored. Pipette resistance was 2–4 Mohm. Then, 10 μM forskolin was added to the extracellular solution, and the cells were perfused for 5 min before recording.

ACKNOWLEDGMENTS. Research reported in this article made use of the Waitt Advanced Biophotonics Center Core Facility [supported by the Waitt Foundation, National Cancer Institute (NCI) Grant P30 CA014195-40, and

National Institute of Neurological Disorders and Stroke Grant P30 NS072031-03], the Histology and Imaging Core Facility, the Flow Cytometry and Functional Genomics Core Facilities (supported by NCI Grant P30 CA014195-40), and the Stem Cell Core Facility [supported by California Institute for Regenerative Medicine (CIRM) Grant CL-1-0500-1 and the Leona M. and Harry B. Helmsley Charitable Trust]. A.L.F. is supported by CIRM Postdoctoral Training Fellowship TG2-01158. C.T.D. (2012) was supported by CIRM-Bridges Internship TB1-01175. I.M.V. is an American Cancer Society Professor of Molecular Biology and holds the Irwin and Joan Jacobs Chair in Exemplary Life Science. This work was supported in part by CIRM Grant CL1-00500-1.2 and the Berger Foundation.

1. Takahashi K, Okita K, Nakagawa M, Yamanaka S (2007) Induction of pluripotent stem cells from fibroblast cultures. *Nat Protoc* 2(12):3081–3089.
2. Wong AP, et al. (2012) Directed differentiation of human pluripotent stem cells into mature airway epithelia expressing functional CFTR protein. *Nat Biotechnol* 30(9): 876–882.
3. Kadzik RS, Morrisey EE (2012) Directing lung endoderm differentiation in pluripotent stem cells. *Cell Stem Cell* 10(4):355–361.
4. Maeda Y, Davé V, Whitsett JA (2007) Transcriptional control of lung morphogenesis. *Physiol Rev* 87(1):219–244.
5. Kumar VH, Lakshminrusimha S, El Abiad MT, Chess PR, Ryan RM (2005) Growth factors in lung development. *Adv Clin Chem* 40:261–316.
6. Weaver M, Yingling JM, Dunn NR, Bellusci S, Hogan BL (1999) Bmp signaling regulates proximal-distal differentiation of endoderm in mouse lung development. *Development* 126(18):4005–4015.
7. Rawlins EL, Ostrowski LE, Randell SH, Hogan BL (2007) Lung development and repair: Contribution of the ciliated lineage. *Proc Natl Acad Sci USA* 104(2):410–417.
8. Kimura J, Deutsch GH (2007) Key mechanisms of early lung development. *Pediatr Dev Pathol* 10(5):335–347.
9. Gontan C, et al. (2008) Sox2 is important for two crucial processes in lung development: Branching morphogenesis and epithelial cell differentiation. *Dev Biol* 317(1):296–309.
10. D'Amour KA, et al. (2005) Efficient differentiation of human embryonic stem cells to definitive endoderm. *Nat Biotechnol* 23(12):1534–1541.
11. Mfopou JK, Chen B, Sui L, Sermon K, Bouwens L (2010) Recent advances and prospects in the differentiation of pancreatic cells from human embryonic stem cells. *Diabetes* 59(9):2094–2101.
12. Green MD, et al. (2011) Generation of anterior foregut endoderm from human embryonic and induced pluripotent stem cells. *Nat Biotechnol* 29(3):267–272.
13. Hyatt BA, Shangguan X, Shannon JM (2004) FGF-10 induces SP-C and Bmp4 and regulates proximal-distal patterning in embryonic tracheal epithelium. *Am J Physiol Lung Cell Mol Physiol* 287(6):L1116–L1126.
14. Lü J, Izvolsky KI, Qian J, Cardoso WV (2005) Identification of FGF10 targets in the embryonic lung epithelium during bud morphogenesis. *J Biol Chem* 280(6):4834–4841.
15. Bellusci S, Grindley J, Emoto H, Itoh N, Hogan BL (1997) Fibroblast growth factor 10 (FGF10) and branching morphogenesis in the embryonic mouse lung. *Development* 124(23):4867–4878.
16. Lebeche D, Malpel S, Cardoso WV (1999) Fibroblast growth factor interactions in the developing lung. *Mech Dev* 86(1-2):125–136.
17. Shiratori M, et al. (1996) Keratinocyte growth factor and embryonic rat lung morphogenesis. *Am J Respir Cell Mol Biol* 15(3):328–338.
18. Geng Y, et al. (2011) Follistatin-like 1 (Fstl1) is a bone morphogenetic protein (BMP) 4 signaling antagonist in controlling mouse lung development. *Proc Natl Acad Sci USA* 108(17):7058–7063.
19. Zhu NL, Li C, Xiao J, Minoo P (2004) NKX2.1 regulates transcription of the gene for human bone morphogenetic protein-4 in lung epithelial cells. *Gene* 327(1):25–36.
20. Di Palma T, et al. (2013) Pax8 has a critical role in epithelial cell survival and proliferation. *Cell Death Dis* 4:e729.
21. Fagman H, et al. (2011) Gene expression profiling at early organogenesis reveals both common and diverse mechanisms in foregut patterning. *Dev Biol* 359(2):163–175.
22. de Jong PM, et al. (1994) Ciliogenesis in human bronchial epithelial cells cultured at the air-liquid interface. *Am J Respir Cell Mol Biol* 10(3):271–277.
23. Vaughan MB, Ramirez RD, Wright WE, Minna JD, Shay JW (2006) A three-dimensional model of differentiation of immortalized human bronchial epithelial cells. *Differentiation* 74(4):141–148.
24. Rock JR, et al. (2011) Notch-dependent differentiation of adult airway basal stem cells. *Cell Stem Cell* 8(6):639–648.
25. Stubbs JL, Davidson L, Keller R, Kintner C (2006) Radial intercalation of ciliated cells during Xenopus skin development. *Development* 133(13):2507–2515.
26. Tsao PN, et al. (2011) Notch signaling prevents mucous metaplasia in mouse conducting airways during postnatal development. *Development* 138(16):3533–3543.
27. Stubbs JL, Vladar EK, Axelrod JD, Kintner C (2012) Multicilin promotes centriole assembly and ciliogenesis during multiciliate cell differentiation. *Nat Cell Biol* 14(2):140–147.
28. Marcet B, Chevalier B, Coraux C, Kodjabachian L, Barbry P (2011) MicroRNA-based silencing of Delta/Notch signaling promotes multiple cilia formation. *Cell Cycle* 10(17): 2858–2864.
29. Jurisch-Yaksi N, et al. (2013) Rer1p maintains ciliary length and signaling by regulating γ-secretase activity and Foxj1a levels. *J Cell Biol* 200(6):709–720.
30. Guseh JS, et al. (2009) Notch signaling promotes airway mucous metaplasia and inhibits alveolar development. *Development* 136(10):1751–1759.
31. Huang SX, et al. (2014) Efficient generation of lung and airway epithelial cells from human pluripotent stem cells. *Nat Biotechnol* 32(1):84–91.
32. Longmire TA, et al. (2012) Efficient derivation of purified lung and thyroid progenitors from embryonic stem cells. *Cell Stem Cell* 10(4):398–411.
33. Cassel TN, Nord M (2003) C/EBP transcription factors in the lung epithelium. *Am J Physiol Lung Cell Mol Physiol* 285(4):L773–L781.
34. Roos AB, Berg T, Barton JL, Didon L, Nord M (2012) Airway epithelial cell differentiation during lung organogenesis requires C/EBPα and C/EBPβ. *Dev Dyn* 241(5): 911–923.
35. Van Haute L, De Block G, Liebaers I, Sermon K, De Rycke M (2009) Generation of lung epithelial-like tissue from human embryonic stem cells. *Respir Res* 10:105.
36. Yamaya M, Finkbeiner WE, Chun SY, Widdicombe JH (1992) Differentiated structure and function of cultures from human tracheal epithelium. *Am J Physiol* 262(6 Pt 1): L713–L724.
37. Neuberger T, Burton B, Clark H, Van Goor F (2011) Use of primary cultures of human bronchial epithelial cells isolated from cystic fibrosis patients for the pre-clinical testing of CFTR modulators. *Methods Mol Biol* 741:39–54.
38. Coyne CB, Gambling TM, Boucher RC, Carson JL, Johnson LG (2003) Role of claudin interactions in airway tight junctional permeability. *Am J Physiol Lung Cell Mol Physiol* 285(5):L1166–L1178.
39. Sears PR, Davis CW, Chua M, Sheehan JK (2011) Mucociliary interactions and mucus dynamics in ciliated human bronchial epithelial cell cultures. *Am J Physiol Lung Cell Mol Physiol* 301(2):L181–L186.
40. Matsui H, Randell SH, Peretti SW, Davis CW, Boucher RC (1998) Coordinated clearance of periciliary liquid and mucus from airway surfaces. *J Clin Invest* 102(6):1125–1131.
41. Gomperts BN, Gong-Cooper X, Hackett BP (2004) Foxj1 regulates basal body anchoring to the cytoskeleton of ciliated pulmonary epithelial cells. *J Cell Sci* 117(Pt 8): 1329–1337.
42. Stubbs JL, Oishi I, Izpisúa Belmonte JC, Kintner C (2008) The forkhead protein Foxj1 specifies node-like cilia in Xenopus and zebrafish embryos. *Nat Genet* 40(12):1454–1460.
43. Jurczyk A, et al. (2004) Pericentrin forms a complex with intraflagellar transport proteins and polycystin-2 and is required for primary cilia assembly. *J Cell Biol* 166(5): 637–643.
44. Jain R, et al. (2010) Temporal relationship between primary and motile ciliogenesis in airway epithelial cells. *Am J Respir Cell Mol Biol* 43(6):731–739.
45. Tsao PN, et al. (2009) Notch signaling controls the balance of ciliated and secretory cell fates in developing airways. *Development* 136(13):2297–2307.
46. Boers JE, Ambergen AW, Thunnissen FB (1999) Number and proliferation of clara cells in normal human airway epithelium. *Am J Respir Crit Care Med* 159(5 Pt 1):1585–1591.
47. Rogers DF (1994) Airway goblet cells: Responsive and adaptable front-line defenders. *Eur Respir J* 7(9):1690–1706.
48. Rose MC, Voynow JA (2006) Respiratory tract mucin genes and mucin glycoproteins in health and disease. *Physiol Rev* 86(1):245–278.
49. Singh G, Katyal SL (1997) Clara cells and Clara cell 10 kD protein (CC10). *Am J Respir Cell Mol Biol* 17(2):141–143.
50. Chen G, et al. (2009) SPDEF is required for mouse pulmonary goblet cell differentiation and regulates a network of genes associated with mucus production. *J Clin Invest* 119(10):2914–2924.
51. Perez-Gil J, Weaver TE (2010) Pulmonary surfactant pathophysiology: Current models and open questions. *Physiology (Bethesda)* 25(3):132–141.
52. Kalina M, Mason RJ, Shannon JM (1992) Surfactant protein C is expressed in alveolar type II cells but not in Clara cells of rat lung. *Am J Respir Cell Mol Biol* 6(6):594–600.
53. Voorhout WF, et al. (1992) Immunocytochemical localization of surfactant protein D (SP-D) in type II cells, Clara cells, and alveolar macrophages of rat lung. *J Histochem Cytochem* 40(10):1589–1597.
54. Rubenstein RC, et al. (2011) Regulation of endogenous ENaC functional expression by CFTR and ΔF508-CFTR in airway epithelial cells. *Am J Physiol Lung Cell Mol Physiol* 300(1):L88–L101.
55. Mou H, et al. (2012) Generation of multipotent lung and airway progenitors from mouse ESCs and patient-specific cystic fibrosis iPSCs. *Cell Stem Cell* 10(4):385–397.
56. Marshall WF (2008) Basal bodies platforms for building cilia. *Curr Top Dev Biol* 85:1–22.
57. Noone PG, et al. (2004) Primary ciliary dyskinesia: Diagnostic and phenotypic features. *Am J Respir Crit Care Med* 169(4):459–467.
58. Morimoto M, et al. (2010) Canonical Notch signaling in the developing lung is required for determination of arterial smooth muscle cells and selection of Clara versus ciliated cell fate. *J Cell Sci* 123(Pt 2):213–224.
59. Coppens JT, Van Winkle LS, Pinkerton K, Plopper CG (2007) Distribution of Clara cell secretory protein expression in the tracheobronchial airways of rhesus monkeys. *Am J Physiol Lung Cell Mol Physiol* 292(5):L1155–L1162.
60. Hovenberg HW, Davies JR, Carlstedt I (1996) Different mucins are produced by the surface epithelium and the submucosa in human trachea: Identification of MUC5AC as a major mucin from the goblet cells. *Biochem J* 318(Pt 1):319–324.
61. Wenzel S, Holgate ST (2006) The mouse trap: It still yields few answers in asthma. *Am J Respir Crit Care Med* 174(11):1173–1176, discussion 1176–1178.
62. Sun X, et al. (2010) Disease phenotype of a ferret CFTR-knockout model of cystic fibrosis. *J Clin Invest* 120(9):3149–3160.
63. Foster KA, Avery ML, Yazdanian M, Audus KL (2000) Characterization of the Calu-3 cell line as a tool to screen pulmonary drug delivery. *Int J Pharm* 208(1-2):1–11.
64. Stewart CE, Torr EE, Mohd Jamili NH, Bosquillon C, Sayers I (2012) Evaluation of differentiated human bronchial epithelial cell culture systems for asthma research. *J Allergy (Cairo)* 2012:943982.
65. Wood AJ, et al. (2011) Targeted genome editing across species using ZFNs and TALENs. *Science* 333(6040):307.